Published in final edited form as:
*J Comput Neurosci*. 2008 April ; 24(2): 195. doi:10.1007/s10827-007-0050-x.

# Influence of Frequency and Temperature on the Mechanisms of Nerve Conduction Block Induced by High-Frequency Biphasic Electrical Current

**Jicheng Wang**, **Bing Shen**, **James R. Roppolo**, **William C. de Groat**, and **Changfeng Tai**
Department of Pharmacology, University of Pittsburgh, Pittsburgh, PA 15261, USA

## Abstract

The influences of stimulation frequency and temperature on mechanisms of nerve conduction block induced by high-frequency biphasic electrical current were investigated using a lumped circuit model of the myelinated axon based on Schwarz and Eikhof (SE) equations. The simulation analysis showed that a temperature-frequency relationship was determined by the axonal membrane dynamics (i.e. how fast the ion channels can open or close.). At a certain temperature, the axonal conduction block always occurred when the period of biphasic stimulation was smaller than the action potential duration (APD). When the temperature decreased from 37°C to 15°C, the membrane dynamics slowed down resulting in an APD increase from 0.4 ms to 2.4 ms accompanied by a decrease in the minimal blocking frequency from 4 kHz to 0.5 kHz. The simulation results also indicated that as the stimulation frequency increased the mechanism of conduction block changed from a cathodal/anodal block to a block dependent upon continuous activation of potassium channels. Understanding the interaction between the minimal blocking frequency and temperature could promote a better understanding of the mechanisms of high frequency induced axonal conduction block and the clinical application of this method for blocking the nerve conduction.

### Keywords

Axon; Block; Model; Temperature; Frequency; Stimulation

## Introduction

Nerve conduction block induced by electrical current has many clinical applications. For example, blocking peripheral nerves could help alleviate chronic pain of peripheral origin (Nashold et al., 1982) or stop unwanted motor effects such as muscle spasms and spasticity (Kilgore and Bhadra, 2004). Blocking pudendal nerve conduction in spinal cord injured people during micturition could reduce urethral sphincter contraction and urethral outlet resistance, and improve voiding efficiency (Tai et al., 2004). A reversible nerve blocking method using biphasic electrical current is more useful than uniphasic current in chronic applications, since the biphasic stimulation causes less tissue damage due to electro-chemical reactions (Agnew and McCreery, 1990). Therefore, recent studies have focused on high-frequency biphasic electrical stimulation (Bhadra and Kilgore, 2005; Bhadra et al., 2006; Tai et al., 2005a,b,c; Williamson and Andrews, 2005; Zhang et al., 2006a,b).

Correspondence to: Changfeng Tai, Ph.D., Department of Pharmacology, University of Pittsburgh, W1354 Biomedical Science Tower, Pittsburgh, PA15261, USA, Phone: 412-648-7016, Fax: 412-648-1945, cftai@pitt.edu.

It has been known for more than 60 years (Reboul and Rosenblueth, 1939; Rosenblueth and Reboul, 1939) that high-frequency biphasic current could block nerve conduction. However, the minimal stimulation frequency required to block nerves varied considerably from 10 kHz to as low as 1 kHz in reports from different investigators (Bhadra et al., 2006; Bhadra and Kilgore, 2005; Bowman and McNeal, 1986; Kilgore and Bhadra, 2004; Rehoul and Rosenblueth, 1939; Rosenblueth and Rehoul, 1939; Tai et al., 2004; 2005c; Tanner, 1962; Williamson and Andrews, 2005). Previous studies indicated that temperature might play a role in this difference in minimal blocking frequency. For example, a study using isolated frog sciatic nerve (Kilgore and Bhadra, 2004) reported that nerve block could be observed at a stimulation frequency as low as 1 kHz at room temperature. Studies using rat sciatic nerves (Bhadra and Kilgore, 2005; Williamson and Andrews, 2005) showed that consistent nerve block could be achieved at stimulation frequencies greater than 10 kHz which was presumably at body temperature near 37 °C. In one of these studies (Williamson and Andrews, 2005) each rat was warmed during the tests by radiant heat from above and a heating pad below. A recent study (Bhadra et al., 2006) using cat pudendal nerve found that nerve block could be observed between 1 kHz and 30 kHz, but the frequency range to induce a complete block varied significantly between animals. Although in this study (Bhadra et al., 2006) the animal's body temperature was maintained between 37 °C and 39 °C using a thermal blanket, the method to control the pudendal nerve temperature was not described after the nerve was exposed for electrode placement. Our previous studies using cats (Tai et al., 2004; 2005c) indicated that at temperatures between 35 °C and 37 °C the minimal stimulation frequency to block the pudendal nerve conduction was 6 kHz. The pudendal nerve temperature in our studies (Tai et al., 2004; 2005c) was controlled by covering the exposed nerve with warm Krebs solution or mineral oil. A minimal blocking frequency of 4–5 kHz was reported in other studies using cat sciatic nerves (Bowman and McNeal, 1986; Rehoul and Rosenblueth, 1939; Rosenblueth and Rehoul, 1939) when the temperature varied between 25 °C and 35 °C (Rehoul and Rosenblueth, 1939; Rosenblueth and Rehoul, 1939), or was undefined (presumably at room temperature 20–25 °C) (Bowman and McNeal, 1986). While the experimental temperature could be a factor that causes the frequency discrepancy, many other factors might also be involved including electrode geometry (bipolar or tripolar), different nerves (sciatic nerve or pudendal nerve), or different species (frog, rat, or cat).

In this study, we used the Schwarz and Eikhof (SE) model (Rattay and Aberham, 1993; Schwarz and Eikhof, 1987) that was based on the properties of rat myelinated axons to further investigate the possible blocking mechanisms and the influences of frequency and temperature on the nerve conduction block induced by high-frequency biphasic electrical current. An understanding of the interaction between temperature and stimulation frequency might provide further insight into the mechanisms underlying this type of nerve block.

## Methods

The nerve model used in this study is shown in Fig. 1. A 40 mm long, myelinated axon is modeled with the inter-node length $\Delta x = 100d$ (where d is the axon diameter). Each node (nodal length: L = 1 μm) is modeled by a membrane capacitance ($c_m$) and a variable membrane resistance ($R_m$). The ionic currents passing through the variable membrane resistance are described by the SE model (see Appendix) (Rattay and Aberham, 1993;Schwarz and Eikhof, 1987). Two monopolar point electrodes (with the indifferent electrode at infinity) are placed at 1 mm distance to the axon (Fig. 1). One is the block electrode at the 25 mm location along the axon, where the high-frequency biphasic rectangular pulses will be delivered (as shown in Fig. 1). The other is the test electrode at the 5 mm location, which will deliver a uniphasic single pulse (pulse width 0.1 ms and intensity varying from 0.3 mA to 2 mA) to evoke an action potential and test whether this action potential can propagate through the site of the block

electrode. The test electrode will always be a cathode (negative pulse), and the block electrode will always deliver biphasic pulses with the cathodal phase first.

We assume that the axon is in an infinite homogeneous medium (resistivity $\rho_e$=300 Ωcm). After neglecting the small influence induced by the presence of the axon in the homogeneous medium, the extracellular potential $V_{e,n}$, at the nth node along the axon can be calculated by:

$$V_{e,n}(t)=\frac{\rho_e}{4\pi}\left[\frac{I_{block}(t)}{\sqrt{(n\Delta x-x_0)^2+z_0^2}}+\frac{I_{test}(t)}{\sqrt{(n\Delta x-x_1)^2+z_1^2}}\right]$$

where $I_{block}(t)$ is the high-frequency biphasic pulse current delivered to the block electrode (at location $x_0$ = 25 mm, $z_0$ = 1 mm); $I_{test}(t)$ is the single test pulse delivered to the test electrode (at location $x_1$ = 5 mm, $z_1$ = 1 mm).

The change of the membrane potential $V_n$ at the $n$ th node is described by:

$$\frac{dV_n}{dt}=\left[\frac{d}{4\rho_i}\left(\frac{V_{n-1}-2V_n+V_{n+1}}{\Delta x^2}+\frac{V_{e,n-1}-2V_{e,n}+V_{e,n+1}}{\Delta x^2}\right)-I_{i,n}\right]/c_m$$

where $V_n = V_{a,n} - V_{e,n} - V_{rest}$; $V_{a,n}$ is the intracellular potential at the $n$ th node; $V_{e,n}$ is the extracellular potential at the $n$ th node; $V_{rest}$ is the resting membrane potential; $d$ is the axon diameter; $\rho_i$ is the resistivity of axoplasm (100 Ωcm); $c_m$ is the capacity of the membrane (2.8 μF/cm$^2$); $I_{i,n}$ is the ionic current at the $n$ th node described by SE equations (see Appendix) (Rattay and Aberham, 1993;Schwarz and Eikhof, 1987).

The SE model was solved by the Runge-Kutta method (Boyce and Diprima, 1997) with a time step of 0.001 ms. The simulation always started at initial condition $V_n$ = 0. The membrane potentials at the two end nodes of the modeled axon were always equal to the membrane potentials of their closest neighbors, which implemented sealed boundary conditions (no longitudinal currents) at the two ends of the modeled axon.

## Results

### A. Nerve Conduction Block Induced by High-Frequency Biphasic Electrical Current

The SE model successfully simulated the conduction block induced by high-frequency biphasic electrical current. As an example, Fig. 2 shows a typical nerve firing pattern and conduction block at different stimulation intensities. In Fig. 2, one axis is the distance along the axon (see Fig. 2A), and the other axis is the time. The locations of the test and block electrodes are marked by short arrows along the axon. The single test pulse and the high-frequency blocking pulses are schematically plotted on the side in Fig. 2A to show the timing of the two different stimulations. With the stimulation intensity below the block threshold as shown in Fig. 2A, the high-frequency blocking stimulation generated an initial action potential (at location 2.5 cm) that propagated in two directions. Then, the high-frequency stimulation alternately depolarized and hyperpolarized the axon membrane without generating action potentials. After a 3 ms delay, an action potential was initiated by the test electrode (at location 0.5 cm) and it propagated through the site of the block electrode (at location 2.5 cm). When the intensity of high-frequency stimulation was increased above the block threshold as shown in Fig. 2B, the action potential initiated by the test electrode was blocked. However, further increasing the intensity of high-frequency stimulation caused repetitive firing as shown in Fig. 2C, although the high-frequency stimulation only induced one action potential at other intensities (Fig. 2A,

B, and D). The repetitive firing of action potentials was continued as long as the blocking stimulation was presented, but within 6 ms as shown in Fig. 2C only 2 action potentials could be plotted. This repetitive firing disappeared and nerve conduction could be blocked again if the stimulation intensity increased further (Fig. 2D).

Fig. 3 shows the pattern of nerve block or repetitive firing at different stimulation frequencies (1–10 kHz) and intensities (0–5 mA) for axons of different diameters (2–20 μm) when the temperature was 37°C. At lower frequencies, the axon could fire repetitively over a larger range of stimulation intensities. However, when the frequency was increased above 5 kHz, the repetitive firing disappeared and the axon could be blocked over a large range of intensities. At frequencies below 5 kHz, there was only a very small range of stimulation intensities where a complete block of the nerve fibers with different diameters could occur. In order to completely block all axons (diameter 2–20 μm) the stimulation frequency must be greater than 5 kHz with stimulation intensity above the blocking threshold.

### B. Mechanism of Nerve Conduction Block at Different Frequency

In order to understand the possible mechanisms of conduction block at different frequencies, we investigated the changes in membrane potential, ionic currents, and activation/inactivation of the ion channels near the block electrode when nerve conduction block occurred. Fig. 4A shows a conduction block occurring at stimulation frequency of 1 kHz. The black frame in Fig. 4A circled the area where nerve block occurred, which included the data from five consecutive nodes at distances 0–4 mm away from the block electrode. The detail membrane activity within the black frame in Fig. 4A is shown in Fig. 4B–G (node at 0 mm was under the block electrode). The propagating action potential from the test electrode was marked by an "*" in Fig. 4B. The membrane depolarizations shown in Fig. 4B that were not marked by an "*" were induced by the 1 kHz blocking stimulation. These depolarizations attenuated in a gradual manner at increasing distances from the blocking electrode (see Fig. 4B). The ionic currents and the activation/inactivation of the ion channels corresponding to the membrane activity shown in Fig. 4B were plotted in Fig. 4C–G. The propagating action potential initiated by the test electrode arrived at the block electrode at about 3.5 ms (see Fig. 4B) when the biphasic blocking current was in the anodal phase. The strong hyperpolarization induced by the anodal pulse under the blocking electrode caused the conduction failure of the action potential (see Fig. 4B, 3.5–4.0 ms). This was further evidenced by the fact that both sodium and potassium currents were zero under the blocking electrode when the action potential arrived (see Fig. 4C and D, 3.5–4.0 ms). The zero sodium current was due to the membrane hyperpolarization that caused the de-activation of sodium channels, i.e. the activation of sodium channels became zero at the blocking electrode (see Fig. 4E, 3.5–4.0 ms). The zero potassium current was caused by the de-activation of potassium channels, i.e. the activation of potassium became zero at the blocking electrode (see Fig. 4G, 3.5–4.0 ms).

In addition to the anodal block shown in Fig. 4, cathodal block could also occur at the frequency of 1 kHz if the propagating action potential arrived at the block electrode when the biphasic blocking current was in the cathodal phase (see Fig. 5A, 3.0–3.5 ms). The strong depolarization at the block electrode induced by the cathodal pulse caused the conduction block of the propagating action potential (see Fig. 5A). The inactivation of sodium channels (h) was changed to zero at the block electrode (see Fig. 5E, 3.0–3.5 ms), although the activation of sodium channels (m) was still high (see Fig. 5D, 3.0–3.5 ms). Thus, when the propagating action potential arrived at the block electrode the sodium current was zero (see Fig. 5B, 3.0–3.5 ms). Meanwhile, the potassium current was large due to the activation of potassium channels (n) (see Fig. 5C and F, 3.0–3.5 ms). Therefore, the conduction block at the frequency of 1 kHz could be induced either by an anodal block (Fig. 4) or by a cathodal block (Fig. 5)

depending on the polarity of high-frequency biphasic current when the action potential arrived at the blocking electrode.

At higher stimulation frequencies, a completely different blocking mechanism was identified. Fig. 6 shows the blocking mechanism at a frequency of 8 kHz. The propagation of the action potential, as well as the sodium and potassium currents associated with the action potential were completely abolished at the node (0 mm) under the blocking electrode where axon membrane was alternately depolarized and hyperpolarized (see Fig. 6A). As the action potential propagated toward the blocking electrode, both the activation (m) and inactivation (h) of sodium channels became oscillatory at the node under the blocking electrode (see Fig. 6D and E) resulting in a pulsed inward sodium current (see Fig. 6B). Therefore, the sodium channels were never completely blocked when conduction block occurred. Activation (n) of potassium channels also became oscillatory at the node under the blocking electrode (see Fig. 6F) resulting in a large pulsed outward potassium current (see Fig. 6C). This large outward potassium current opposed the large inward sodium current, which caused the node under the block electrode to become un-excitable leading to the block of action potential propagation. Therefore, the mechanism of conduction block at higher frequencies was due to the activation of potassium channels under the blocking electrode. For the purpose of discussion in this paper, this blocking mechanism will be termed “potassium block”.

The mechanism of conduction block changed from an anodal/cathodal block to a potassium block as the stimulation frequency increased from 1 kHz to 10 kHz. Fig. 7 shows how activation (n) of potassium channels under the blocking electrode changed when the frequency increased. At the frequency of 1 kHz, the activation (n) of potassium channels changed between 0 and 0.75 with either an anodal or a cathodal block (see Fig. 4 and Fig. 5). When the frequency increased above 4 kHz, the activation (n) of potassium channels began to oscillate at a level above zero resulting in a potassium block as shown in Fig. 6.

### C. Blocking Mechanism Changes with Temperature

The potassium block could also occur at the frequency of 1 kHz if the temperature was low. Fig. 8 shows the mechanism of nerve conduction block induced by 1 kHz stimulation at 20° C. The blocking mechanism was the same as the potassium block induced at 8 kHz and 37°C (see Fig. 6). It was very different from the anodal/cathodal block shown in Fig. 4 and Fig. 5. Therefore, the mechanism of nerve conduction block for 1 kHz stimulation changed from an anodal/cathodal block to a potassium block as the temperature changed from 37°C to 20°C.

Fig. 9 shows the influence of temperature on the activation (n) of potassium channels at the node under the blocking electrode. When the temperature decreased from 37°C to below 20° C, the activation (n) of potassium channels became oscillating at a level above zero resulting in a change in the mechanism of conduction block from an anodal/cathodal block to a potassium block.

### D. Relationship between Temperature, Action Potential Duration (APD), and Minimal Blocking Frequency for Potassium Block

The relationship between temperature, APD and the minimal stimulation frequency to induce a potassium block was also examined. As the temperature decreased from 37°C to 15°C, the APD increased (Fig. 10A) and the activation of potassium channels became slow (Fig. 10B). Meanwhile, at lower temperatures potassium block occurred at a lower stimulation frequency (see Fig. 8 and Fig. 9). For a certain temperature there was a correlation between the APD and a corresponding minimal blocking frequency to induce the potassium block (see Fig. 11A). The minimal blocking frequency to induce potassium block at a certain temperature was identified by investigating the blocking mechanism at every stimulation frequency as shown

in Figs.4–6. Fig. 11B shows the same data as Fig. 11A, but the stimulation frequency was converted to stimulation period. The diagonal dashed line in Fig. 11B indicates where the stimulation period equals APD. In order to induce a potassium block at each temperature, the stimulation period had to be slightly smaller than the APD (see Fig. 11B).

## Discussion

This simulation study employing a myelinated axonal model based on SE equations investigated the nerve conduction block induced by high-frequency biphasic electrical current. Several possible nerve blocking mechanisms were identified including anodal block (Fig. 4), cathodal block (Fig. 5), and potassium block (Fig. 6). At a temperature of 37°C, the blocking mechanism changed from an anodal/cathodal block to a potassium block as the stimulation frequency increased from 1 kHz to 10 kHz (see Fig. 7). However, as the temperature decreased below 20°C, potassium block could be observed at a frequency as low as 1 kHz (see Fig. 8–9). There is a one-to-one relationship between the temperature and the minimal stimulation frequency to induce a potassium block (see Fig. 11).

The temperature-frequency relationship of potassium block is determined by the axonal membrane dynamics (i.e. how fast the ion channels can open or close.). In order to induce a potassium block, the stimulation period must be slightly shorter than the APD (see Fig. 11B), which means that the stimulation has to change its polarity at least once during the time when an action potential propagates through the blocking electrode. At a lower temperature the axonal membrane dynamics become slow resulting in a longer APD (see Fig. 10) and a longer time for an action potential to propagate through the region of the blocking electrode, thereby allowing the period of blocking stimulation to be longer or the frequency to be lower. Meanwhile, the slowed membrane dynamics at a lower temperature also gives the blocking stimulation the ability to maintain the potassium channels open at a lower stimulation frequency (see Fig. 9) resulting in a potassium block.

This simulation study indicated that a temperature change from 37°C to 15°C could result in a shift in the minimal blocking frequency from 4 kHz to 0.5 kHz (see Fig. 11). However, previous studies using animals (Bhadra et al., 2006;Bhadra and Kilgore, 2005;Bowman and McNeal, 1986;Kilgore and Bhadra, 2004;Rehoul and Rosenblueth, 1939;Rosenblueth and Rehoul, 1939;Tai et al., 2004;2005c;Tanner, 1962;Williamson and Andrews, 2005) showed that the minimal blocking frequency varied between 1 kHz and 10 kHz in different nerves of various species using different electrode geometries. Therefore, the temperature might be one of the factors that could influence the minimal blocking frequency. Many other factors might also be involved including electrode geometry (bipolar or tripolar), different nerves (sciatic nerve or pudendal nerve), or different species (frog, rat, or cat). Further studies on these possible influencing factors are needed.

Our simulation analysis suggested that the constant activation of the potassium channels during high-frequency biphasic electrical stimulation (Fig. 6–9) is a possible mechanism underlying the nerve conduction block. A recent study (Bikson et al., 2001) in rat hippocampal slices showed that the neuronal epileptiform activity could be blocked by high frequency (<500 Hz) sinusoidal electrical field stimulation. The block of spontaneous neuronal activity was always coincident with a stimulus-induced rise in extracelluar potassium concentration, suggesting that a constant potassium outflow from the neurons was induced by the stimulation. The stimulation frequency to block the hippocampal neuron is relatively low (<500 Hz) compared to the minimal stimulation frequency required to block the axonal conduction (1–10 kHz) (Bhadra et al., 2006;Bhadra and Kilgore, 2005;Bowman and McNeal, 1986;Kilgore and Bhadra, 2004;Rehoul and Rosenblueth, 1939;Rosenblueth and Rehoul, 1939;Tai et al., 2004; 2005c;Tanner, 1962;Williamson and Andrews, 2005). However, this frequency discrepancy

might be caused by the slow membrane dynamics of the neuron and the longer duration action potential. Our results (Fig. 8–11) have shown that a lower stimulation frequency is required to block the nerve when the membrane dynamics become slower. The duration of the action potential generated in neurons can be several milliseconds long (Renganathan et al, 2001), but it is less than 1 ms in myelinated axons at temperatures above 25 °C. Based on our simulation results and the recent study in rat hippocampal neurons (Bikson et al., 2001), a further investigation on the potassium channels during high-frequency electrical stimulation of the neural tissue is warranted.

The mechanisms of nerve conduction block presented in this study need to be further confirmed by both animal studies and simulation analysis. Although it will be very difficult for studies using animals to verify the details of the blocking mechanism due to technical issues, simulation analysis using other axonal membrane models could be performed. These models include HH model (Hodgkin and Huxley, 1952), FH model (Frankenhaeuser and Huxley, 1964), CRRSS model (Chiu et al., 1979), SRB model (Schwarz et al., 1995), or MRG model (McIntyre et al., 2002), which are derived from the axon membranes of different species (squid, frog, rat, rabbit, or human). Simulation analysis using these axonal models may further reveal that different types of axons (unmyelinated, myelinated, amphibian, or mammalian) may have different blocking frequencies and different mechanisms of block. The mammalian myelinated axon is different from the amphibian myelinated axon in terms of the nodal potassium current. In the amphibian (frog) myelinated axon (Frankenhaeuser and Huxley, 1964), there is large fast potassium current at the node of Ranvier. But in the mammalian myelinated axon the nodal potassium current is very small and mainly consists of a slow potassium current (Roper and Schwarz, 1989; Schwarz et al., 2006). The SE model (Rattay and Aberham, 1993; Schwarz and Eikhof, 1987) used in this study only incorporated a small fast potassium current. Simulation studies using SRB model (Schwarz et al., 1995) or MRG model (McIntyre et al., 2002) which incorporate a slow potassium current are needed in order to evaluate the role of this slow potassium current. However, it is worth noting that this study indicates that the fast potassium current, although it is very small in the mammalian myelinated axon, could play a critical role in the nerve conduction block induced by high-frequency biphasic electrical stimulation. Our previous studies using unmyelinated axon (HH model) (Tai et al., 2005a,b) and amphibian myelinated axon model (FH model) (Zhang et al., 2006a,b), which incorporated only fast potassium current, also showed that the fast potassium current plays a critical role. Furthermore, our study using the CRRSS model (Zhang et al., 2006b), which was derived from mammalian (rabbit) myelinated axon and did not incorporate any potassium current (Chiu et al., 1979), completely failed to simulate the nerve conduction block, further indicating a role of the potassium current. Although the small fast potassium current at the node of Ranvier of the mammalian myelinated nerve may be of importance in nerve conduction block, investigating the role of the slow potassium current is definitively warranted due to its dominant presence at the node of Ranvier (Roper and Schwarz, 1989; Schwarz et al., 2006).

The axonal model used in this study only incorporated ion channel dynamics. Therefore, it can only reveal the possible mechanisms of nerve conduction block due to activation, inactivation, or deactivation of the ion channels. More complex axonal models could be developed which incorporate a more realistic extracellular space, glial buffering, and ion pumps (Kager et al., 2000, 2002; Bazhenov et al., 2004). The glial buffering and ion pump mechanisms could influence the intracellular and extracellular ion concentrations, especially the potassium concentration. It is possible that the high-frequency blocking stimulation modulates the glial buffering or ion pump resulting in a nerve conduction failure. Furthermore, due to the kHz stimulation the Joule heating effect might start to play a role, although a recent theoretical analysis (Elwassif et al., 2006) showed that it is negligible at frequency of 185 Hz during deep brain stimulation. A more realistic axonal model may reveal other nerve blocking mechanisms.

Computer simulation studies using more complex models are needed since these possible mechanisms will be very difficult to evaluate in animal experiments.

A reversible nerve conduction block method will find many applications in both clinical medicine and basic neuroscience (Kilgore and Bhadra, 2004; Nashold et al., 1982; Tai et al., 2004). Understanding the biophysics and mechanisms underlying the nerve conduction block induced by high-frequency biphasic electrical current could promote its clinical application and possibly the design of new stimulation waveforms of a lower frequency to block nerve conduction.

## Acknowledgments

This work is supported by the NIH under grants 1R01-DK-068566-01 and 1R01-NS-051671-01A1.

## References

Agnew, WF.; McCreery, DH. Neural Prostheses: Fundamental Studies. Prentice Hall; Englewood Cliffs, NJ: 1990.

Bazhenov M, Timofeev I, Steriade M, Sejnowski TJ. J Neurophysiol 2004;92:1116–1132. [PubMed: 15056684]

Bhadra N, Bhadra N, Kilgore KL, Gustafson KJ. High frequency electrical conduction block of pudendal nerve. J Neural Eng 2006;3:180–187. [PubMed: 16705274]

Bhadra N, Kilgore KL. High-frequency electrical conduction block of mammalian peripheral motor nerve. Muscle Nerve 2005;32:782–790. [PubMed: 16124008]

Bikson M, Lian J, Hahn PJ, Stacey WC, Sciortino C, Durand DM. Suppression of epileptiform activity by high frequency sinusoidal fields in rat hippocampal slices. J Physiol 2001;531:1810191.

Bowman BR, McNeal DR. Response of single alpha motoneurons to high frequency pulse train: firing behavior and conduction block phenomenon. Appl Neurophysiol 1986;49:121–138. [PubMed: 3827239]

Boyce, WE.; Diprima, RC. Elementary Differential Equations and Boundary Value Problems. 6. John Wiley & Sons, Inc; 1997.

Chiu SY, Ritchie JM, Rogart RB, Stagg D. A quantitative description of membrane currents in rabbit myelinated nerve. J Physiol (Lond) 1979;292:149–166. [PubMed: 314974]

Elwassif MM, Kong Q, Vazquez M, Bikson M. Bio-heat transfer model of deep brain stimulation-induced temperature changes. J Neural Eng 2006;3:306–315. [PubMed: 17124335]

Frankenhaeuser B, Huxley AF. The action potential in the myelinated nerve fibre of Xenopus Laevis as computed on the basis of voltage clamp data. J Physiol (Lond) 1964;171:302–315. [PubMed: 14191481]

Hodgkin AL, Huxley AF. A quantitative description of membrane current and its application to conduction and excitation in nerve. J Physio (Lond) 1952;117:500–544.

Kager H, Wadman WJ, Somjen GG. Simulated seizures and spreading depression in a neuron model incorporating interstitial space and ion concentrations. J Neurophysiol 2000;84:495–512. [PubMed: 10899222]

Kager H, Wadman WJ, Somjen GG. Condition for the triggering of spreading depression studied with computer simulations. J Neuorphysiol 2002;88:2700–2712.

Kilgore KL, Bhadra N. Nerve conduction block utilising high-frequency alternating current. Med Biol Eng Comput 2004;42:394–406. [PubMed: 15191086]

McIntyre CC, Richardson AG, Grill WM. Modeling the excitability of mammalian nerve fibers: Influence of afterpotentials on the recovery cycle. J Neurophysiol 2002;87:995–1006. [PubMed: 11826063]

Nashold BS, Goldner JL, Mullen JB, Bright DS. Long-term pain control by direct peripheral-nerve stimulation. J Bone and Joint Surg 1982;64A:1–10. [PubMed: 6976348]

Rattay F, Aberham M. Modeling axon membranes for functional electrical stimulation. IEEE Trans Biomed Eng 1993;40:1201–1209. [PubMed: 8125496]

Reboul J, Rosenblueth A. The action of alternating currents upon the electrical excitability of nerve. Am J Physiol 1939;125:205–215.

Renganathan M, Cummins TR, Waxman SG. Contribution of $Na_V$ 1.8 sodium channels to action potential electrogenesis in DRG neurons. J Neurophysiol 2001;86:629–640. [PubMed: 11495938]

Roper J, Schwarz JR. Heterogeneous distribution of fast and slow potassium channels in myelinated rat nerve fibres. J Physiol 1989;416:93–110. [PubMed: 2558178]

Rosenblueth A, Reboul J. The blocking and deblocking effects of alternating currents on nerve. Am J Physiol 1939;125:251–264.

Schwarz JR, Eikhof G. Na currents and action potentials in rat myelinated nerve fibres at 20 and 37°C. Pflugers Arch 1987;409:569–577. [PubMed: 2442714]

Schwarz JR, Glassmeier G, Cooper EC, Kao TC, Nodera H, Tabuena D, Kaji R, Bostock H. KCNQ channels mediate $I_{ks}$, a slow $K^+$ current regulating excitability in the rat node of Ranvier. J Physiol 2006;573:17–34. [PubMed: 16527853]

Schwarz JR, Reid G, Bostock H. Action potentials and membrane currents in the human node of Ranvier. Pflugers Arch 1995;430:283–292. [PubMed: 7675638]

Tai C, de Groat WC, Roppolo JR. Simulation analysis of conduction block in unmyelinated axons induced by high-frequency biphasic electrical currents. IEEE Trans Biomed Eng 2005a;52:1323–1332. [PubMed: 16041996]

Tai C, de Groat WC, Roppolo JR. Simulation of nerve block by high-frequency sinusoidal electrical current based on the Hodgkin-Huxley model. IEEE Trans Neural Syst Rehab Eng 2005b;13:415–422.

Tai C, Roppolo JR, de Groat WC. Block of external urethral sphincter contraction by high frequency electrical stimulation of pudendal nerve. J Urol 2004;172:2069–2072. [PubMed: 15540791]

Tai C, Roppolo JR, de Groat WC. Response of external urethral sphincter to high frequency biphasic electrical stimulation of pudendal nerve. J Urol 2005c;174:782–786. [PubMed: 16006976]

Tanner JA. Reversible blocking of nerve conduction by alternating-current excitation. Nature 1962;195:712–713. [PubMed: 13919574]

Williamson RP, Andrews BJ. Localized electrical nerve blocking. IEEE Trans Biomed Eng 2005;52:362–370. [PubMed: 15759566]

Zhang X, Roppolo JR, de Groat WC, Tai C. Simulation analysis of conduction block in myelinated axons induced by high-frequency biphasic rectangular pulses. IEEE Trans Biomed Eng 2006a;53:1433–1436. [PubMed: 16830949]

Zhang X, Roppolo JR, de Groat WC, Tai C. Mechanism of Nerve Conduction Block Induced by High-Frequency Biphasic Electrical Currents. IEEE Trans Biomed Eng 2006b;53:2445–2454. [PubMed: 17153201]

## Appendix

The ionic current $I_{i,,n}$ at nth node is described as:

$$
\begin{aligned}
&I_{i,n}=i_{Na}+i_K+i_L\\
&i_{Na}=P_{Na}m^3h\frac{EF^2}{RT}\frac{[Na]_0-[Na]_ie^{EF/RT}}{1-e^{EF/RT}}\\
&i_K=P_Kn^2\frac{EF^2}{RT}\frac{[K]_0-[K]_ie^{EF/RT}}{1-e^{EF/RT}}\\
&i_L=g_L(V_n-V_L)\\
&E=V_n+V_{rest}
\end{aligned}
$$

where $P_{Na}$ (0.00328 cm/s) and $P_K$ (0.000134 cm/s) are the ionic permeabilities for sodium and potassium currents respectively; $g_L$ (86 $k\Omega^{-1}$ $cm^{-2}$) is the maximum conductance for leakage current. $V_L$ (0 mV) is the reduced equilibrium membrane potential for leakage ions, in which the resting membrane potential $V_{rest}$ (−78 mV) has been subtracted. $[Na]_i$ (8.71 mmole/l) and $[Na]_o$ (154 mmole/l) are sodium concentrations inside and outside the axon membrane. $[K]_i$ (155 mmole/l) and $[K]_o$ (5.9 mmole/l) are potassium concentrations inside and outside the axon membrane. F (96485 C/mole) is Faraday constant. R (8314.4 mJ/K/mole) is gas constant. m,

h and n are dimensionless variables, whose values always change between 0 and 1. m and h represent activation and inactivation of sodium channels, whereas n represents activation of potassium channels.

The evolution equations for m, h and n are the following:

$$dm/dt=[\alpha_m(1-m)-\beta_m m]k_m$$
$$dh/dt=[\alpha_h(1-h)-\beta_h h]k$$
$$dn/dt=[\alpha_n(1-n)-\beta_n n]k$$

and

$$\alpha_m=\frac{1.87(V_n-25.41)}{1-\exp(\frac{25.41-V_n}{6.06})}$$
$$\beta_m=\frac{3.97(21-V_n)}{1-\exp(\frac{V_n-21}{9.41})}$$
$$\alpha_h=-\frac{0.55(V_n+27.74)}{1-\exp(\frac{V_n+27.74}{9.06})}$$
$$\beta_h=\frac{22.6}{1+\exp(\frac{56-V_n}{12.5})}$$
$$\alpha_n=\frac{0.13(V_n-35)}{1-\exp(\frac{35-V_n}{10})}$$
$$\beta_n=\frac{0.32(10-V_n)}{1-\exp(\frac{V_n-10}{10})}$$
$$k_m=2.2^{(T-310)/10}$$
$$k=3^{(T-310)/10}$$

where T is the temperature used in the simulation study (in °Kelvin). The initial values for m, h and n (when $V_n$ = 0 mV) are 0.0077, 0.76 and 0.0267 respectively.

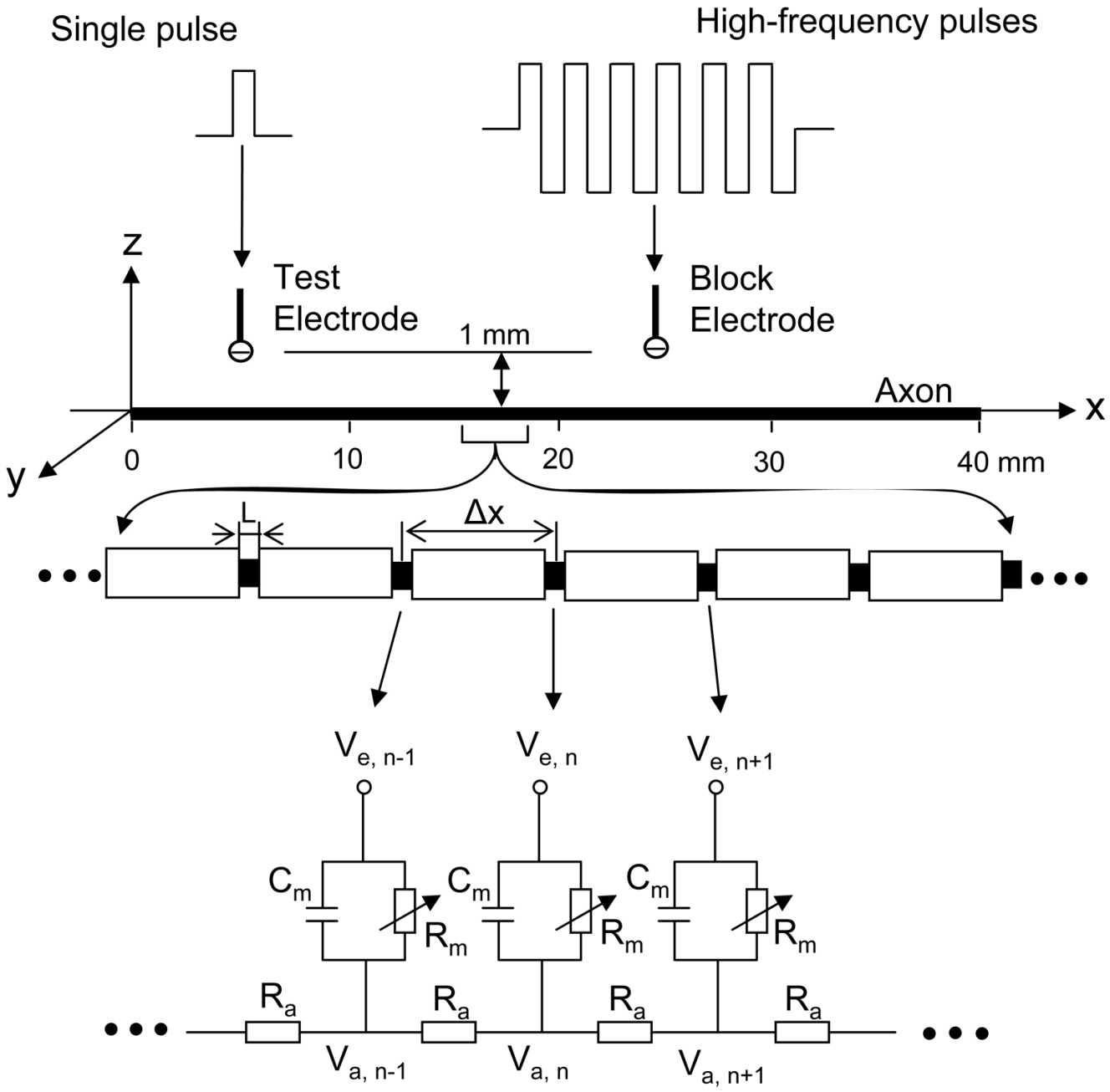


**Fig. 1.**

Axonal model to simulate conduction block induced by high-frequency biphasic electrical current. The inter-node length Δx = 100d; d is the axon diameter. L is the nodal length. Each node is modeled by a resistance-capacity circuit based on SE model. Ra: axoplasm resistance; Rm: membrane resistance; Cm: membrane capacitance; Va: intracellular potential; Ve: extracellular potential; Single pulse: 0.3–2 mA intensity, 0.1 ms pulse width; High-frequency pulses: 0–5 mA intensity, 1–10 kHz frequency.

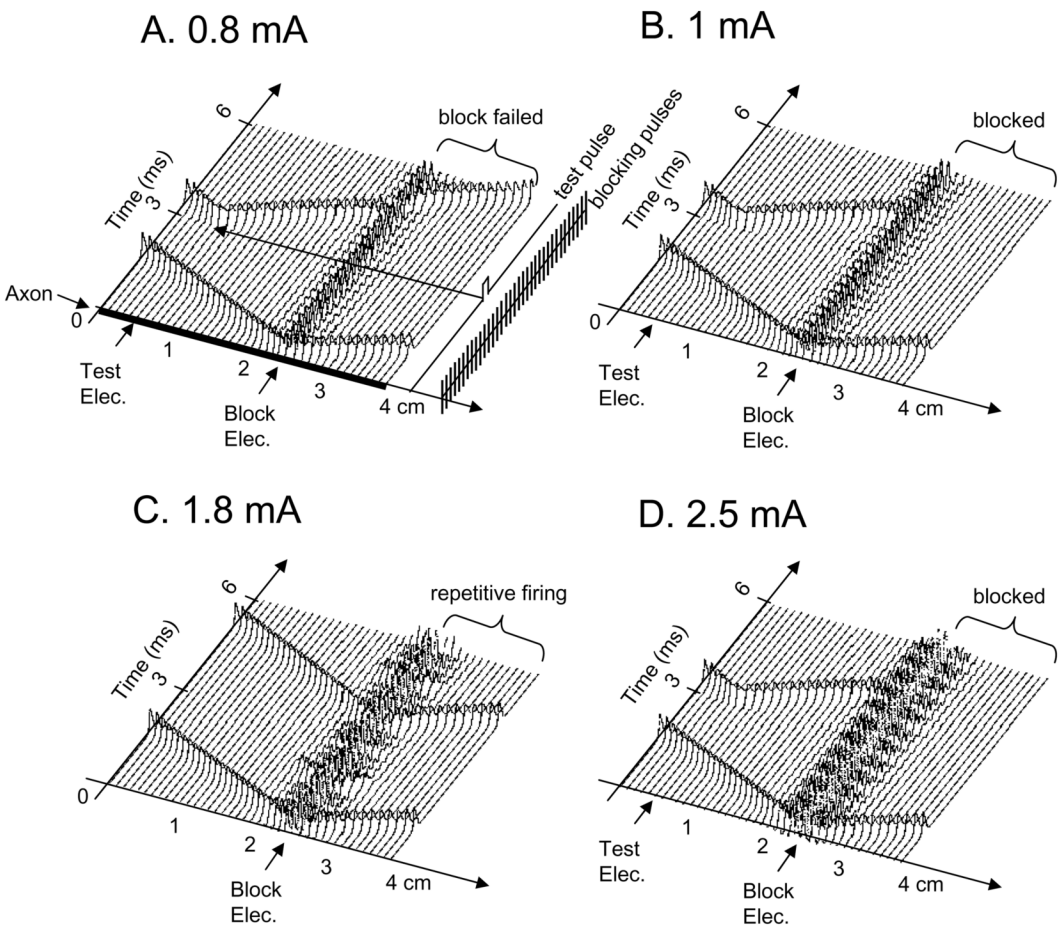


**Fig. 2.**

Propagation of action potentials along an axon induced by high-frequency biphasic stimulation at different intensities. A. 0.8 mA; B. 1 mA; C. 1.8 mA; D. 2.5 mA. In A, B and D, the high-frequency biphasic stimulation only induced an initial action potential, but in C it caused repetitive firing. A second action potential was also initiated after a 3 ms delay by the test electrode in A, B and D, but not in C. This action potential propagated towards the block electrode, and was blocked by the block electrode in B and D, but not in A. The axon is shown in A and the short arrows mark the locations of test and block electrodes along the axon. The test and blocking pulses are also schematically plotted on the side in A to show the timing of the stimulations. Stimulation: 4 kHz. Axon diameter: 5 μm. Temperature: 37 °C.

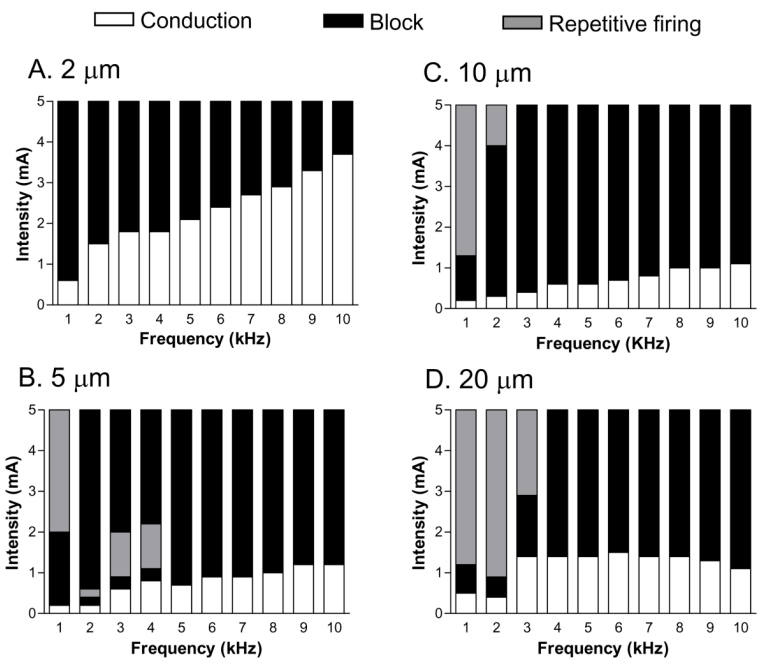


**Fig. 3.**

Pattern of nerve block and repetitive firing at different stimulation frequencies and intensities for axons of different diameters. A. 2 μm; B. 5 μm; C. 10 μm; D. 20 μm. The dark areas represent the stimulation intensity ranges causing nerve block as shown in Fig. 2B or D. The gray areas represent the repetitive firing as shown in Fig. 2C. The white areas represent normal conduction as shown in Fig. 2A. Temperature: 37°C.

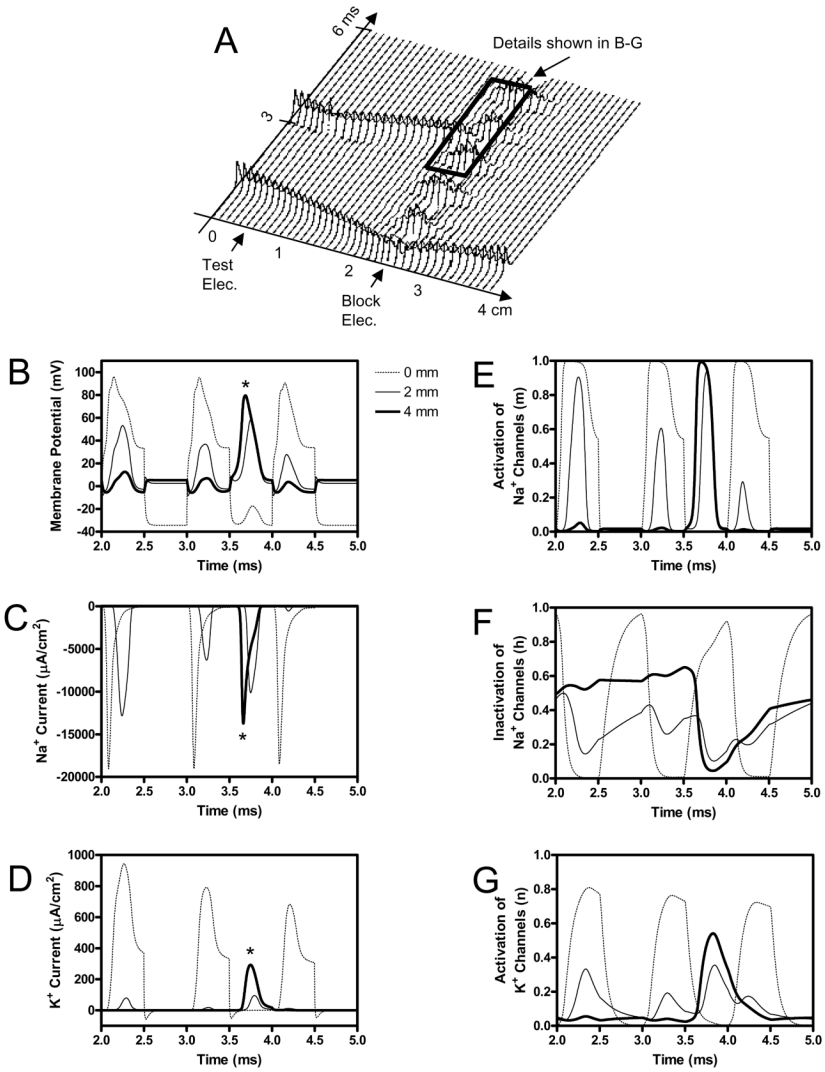


**Fig. 4.**

Propagation of membrane potentials, ionic currents and activation/inactivation of the ion channels near the block electrode when an anodal block occurs. The legends in B indicate the distances from the block electrode (0 mm is under the block electrode). Stimulation: frequency 1 kHz, intensity 0.4 mA. Temperature: 37°C. Axon diameter: 10 μm. The "*" in B, C, and D mark the propagating action potential from the test electrode, and its corresponding ionic currents.

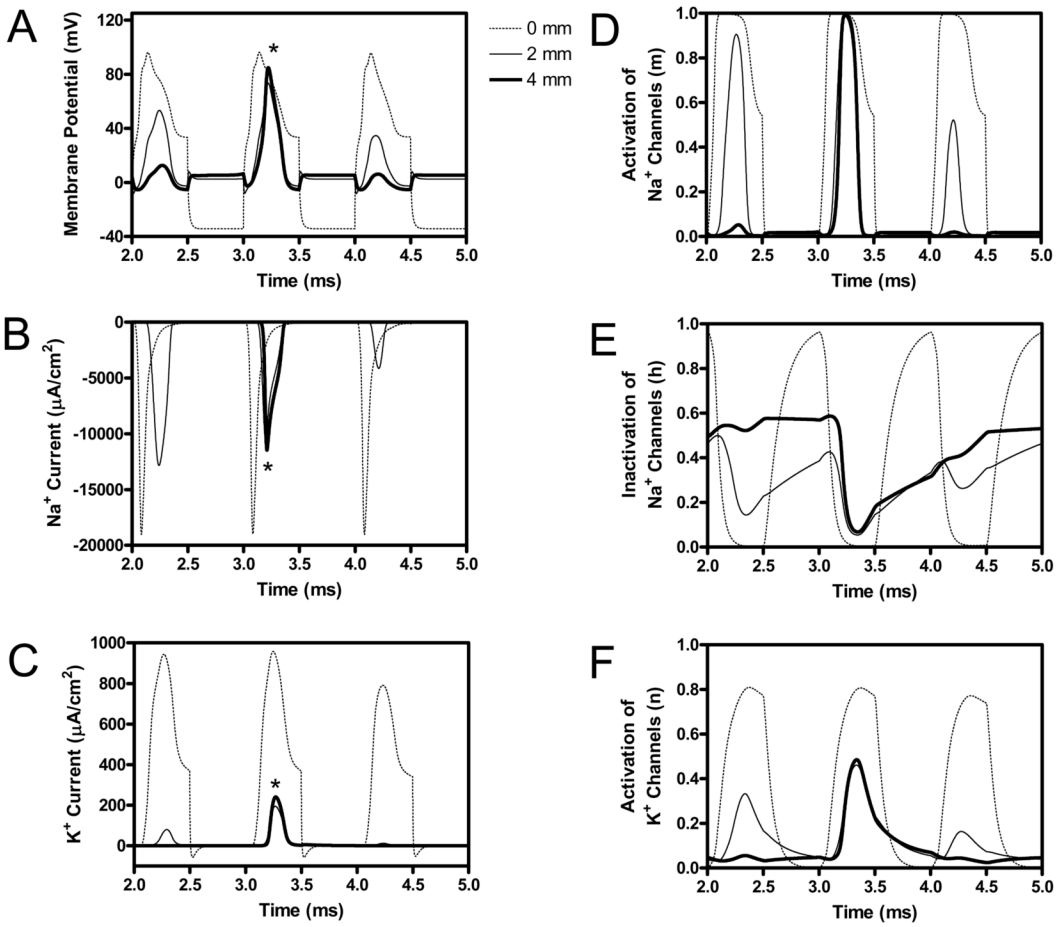


**Fig. 5.**

Propagation of membrane potentials, ionic currents and activation/inactivation of the ion channels near the block electrode when a cathodal block occurs. The legends indicate the distances from the block electrode (0 mm is under the block electrode). Stimulation: frequency 1 kHz, intensity 0.4 mA. Temperature: 37°C. Axon diameter: 10 μm. The "*" in A, B, and C mark the propagating action potential from the test electrode, and its corresponding ionic currents.

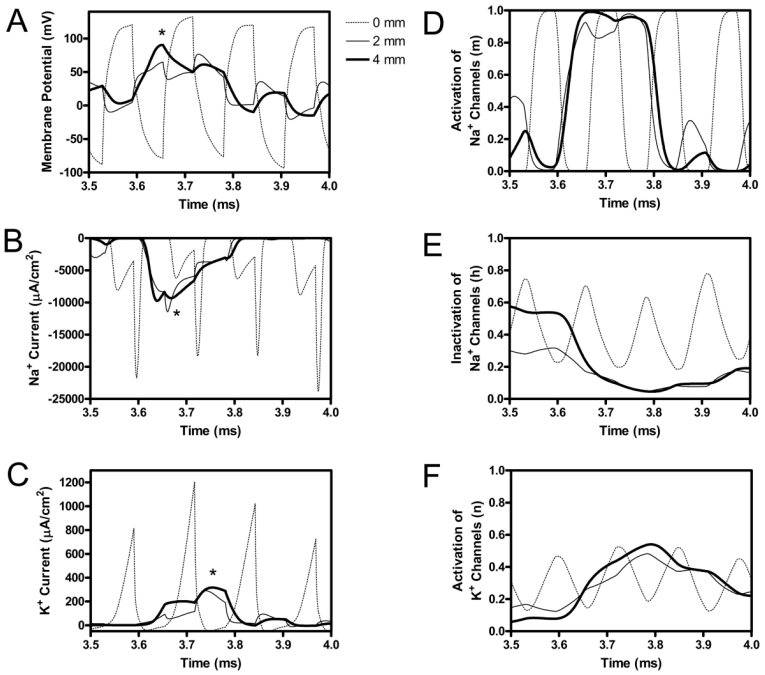


**Fig. 6.**

Propagation of membrane potentials, ionic currents and activation/inactivation of the ion channels near the block electrode when a potassium block occurs. The legends indicate the distances from the block electrode (0 mm is under the block electrode). Stimulation: frequency 8 kHz, intensity 1.2 mA. Temperature: 37°C. Axon diameter: 10 μm. The "*" in A, B, and C mark the propagating action potential from the test electrode, and its corresponding ionic currents.

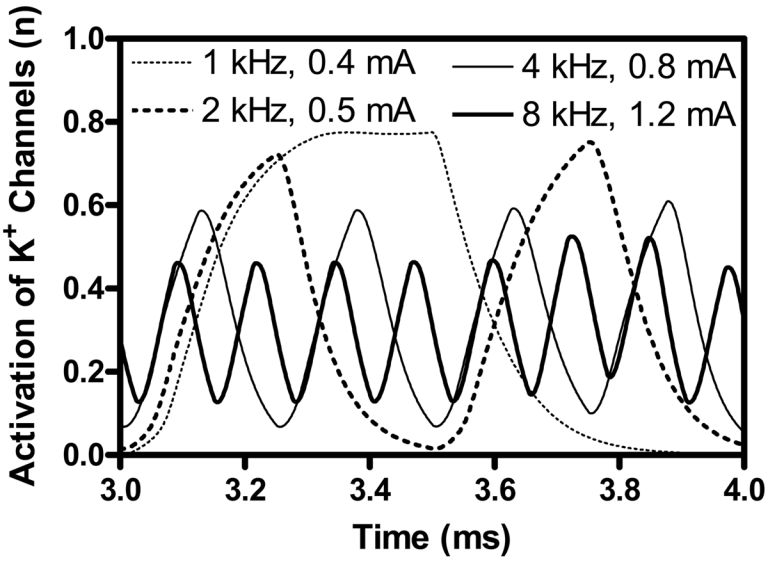


**Fig. 7.**

Change of activation (n) of potassium channels with stimulation frequency under the block electrode. The stimulation intensities are at the blocking threshold levels. Temperature: 37°C. Axon diameter: 10 μm.

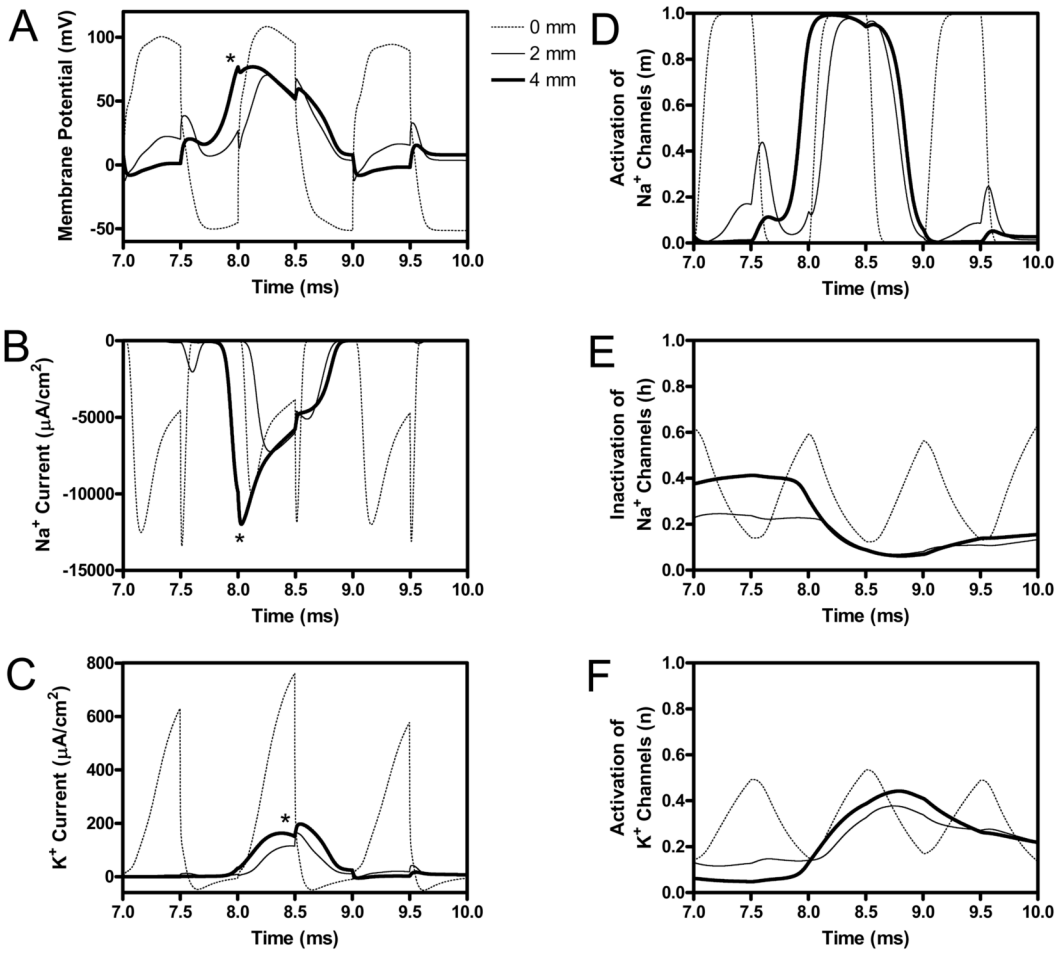


**Fig. 8.**

Propagation of membrane potentials, ionic currents and activation/inactivation of the ion channels near the block electrode when a potassium block occurs. The legends indicate the distances from the block electrode (0 mm is under the block electrode). Stimulation: frequency 1 kHz, intensity 0.6 mA. Temperature: 20°C. Axon diameter: 10 μm. The "*" in A, B, and C mark the propagating action potential from the test electrode, and its corresponding ionic currents.

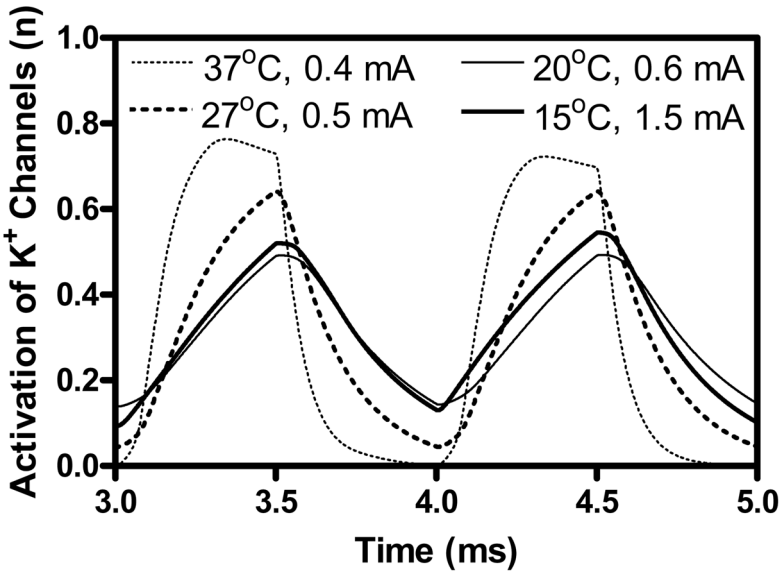


**Fig. 9.**

Change of activation (n) of potassium channels with temperature under the block electrode. The stimulation intensities are at the threshold levels of potassium block. Axon diameter: 10 μm. Stimulation: 1 kHz.

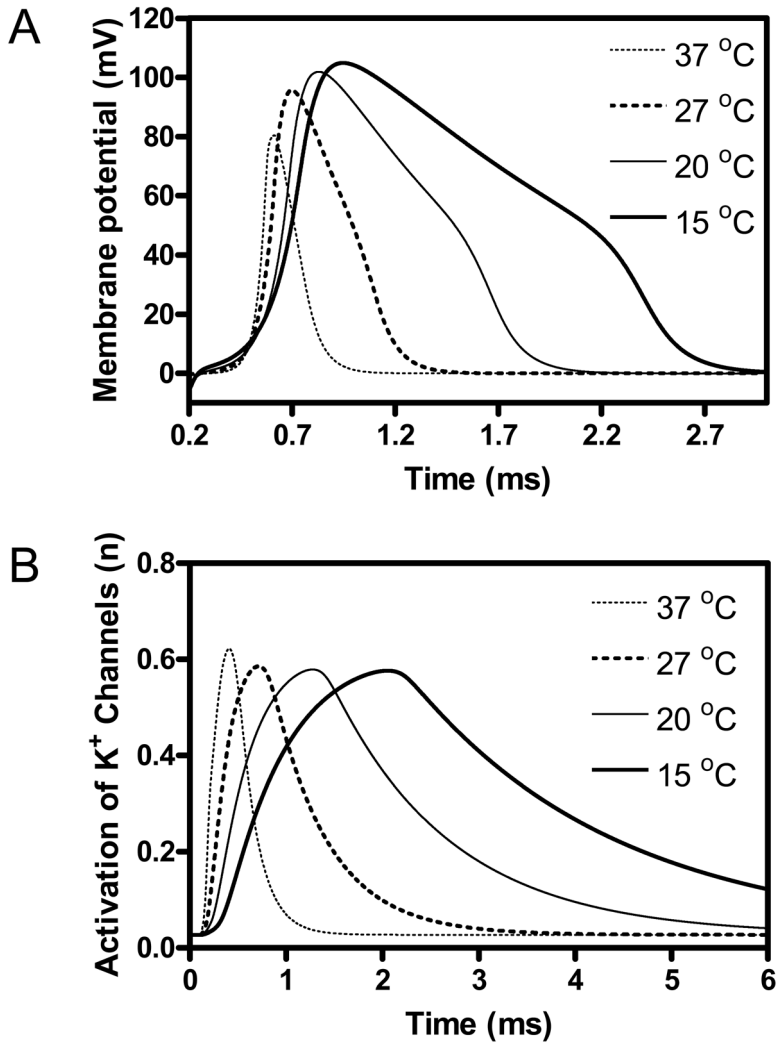


**Fig. 10.**
Change of action potential (A) and activation of $K^+$ channels (B) with temperature.

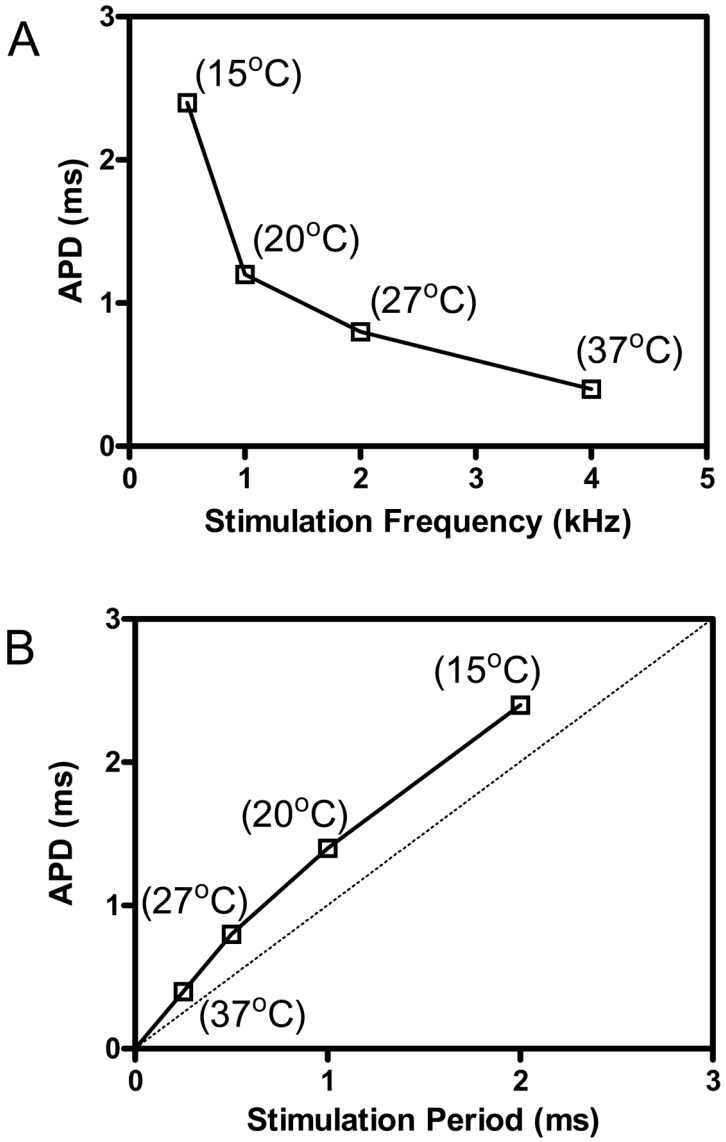


**Fig. 11.**

A: Relationship between action potential duration (APD) and minimal blocking frequency required to induce the potassium block at different temperatures. B: The data are the same as shown in A, but the stimulation frequency is converted to stimulation period. The diagonal dashed line in B indicates where the stimulation period equals to APD.